Takegami et al., Pharm Anal Acta 2015, 6:2
DOI: 10.4172/2153-2435.1000339

Pharmaceutica Analytica Acta

Research Article Open Access

Application of ^{19}F NMR Spectroscopy Using a Novel a–Tocopherol Derivative as a ^{19}F NMR Probe for a Pharmacokinetic Study of Lipid Nano-Emulsions in Mice

Takegami S[1*], Katsumi H[2], Asai K[1], Fujii D[1], Fujimoto T[1], Kawakami H[1], Tokuyama T[1], Konishi A[1], Yamamoto A[2] and Tatsuya Kitade[1]

[1]*Department of Analytical Chemistry, Kyoto Pharmaceutical University, 5 Nakauchicho, Misasagi, Yamashina-ku, Kyoto 607-8414, Japan*
[2]*Department of Biopharmaceutics, Kyoto Pharmaceutical University, 5 Nakauchicho, Misasagi, Yamashina-ku, Kyoto 607-8414, Japan*

Abstract

Objective: The aim of our study was to demonstrate the usefulness of ^{19}F nuclear magnetic resonance (NMR) spectroscopy as an analytical technique applicable for the pharmacokinetic studies of lipid nano-emulsions (LNEs) using a mixture of soybean oil, phosphatidylcholine and sodium palmitate as drug carriers.

Methods: An α−tocopherol derivative, ^{19}F-TP, in which a 4-(trifluoromethyl) benzoyl group was introduced to the hydroxyl group of α-tocopherol was newly synthesized as a ^{19}F NMR probe. Three different LNEs containing ^{19}F-TP, denoted ^{19}F-TP-LNEs (Small-LNE, Large-LNE, and polyethylene glycol-modified LNE (PEG-LNE)) were prepared by the sonication method and characterized using a dynamic light-scattering method and zeta potential analysis. The concentrations of the three ^{19}F-TP-LNEs in the blood, liver and kidney of mice were periodically evaluated based on the ^{19}F NMR signal intensity ratio of ^{19}F-TP using 0.1 mM of trifluoromethane sulfonic acid sodium salt as an internal reference.

Results: ^{19}F-TP was easily synthesized with a high yield of 96% in a one-step procedure. Small-LNE, Large-LNE and PEG-LNE had the mean particle sizes of 58, 157 and 174 nm and zeta potentials of –34, –53 and –32 mV, respectively. A single signal attributable to ^{19}F-TP in ^{19}F-TP-LNEs was observed at 15.4 ppm in the ^{19}F NMR spectra of biological samples, but was observed to decrease over time. From the change of ^{19}F NMR signal of ^{19}F-TP in biological samples, it was shown that three ^{19}F-TP-LNEs had different pharmacokinetic characteristics because of their droplet sizes and surface physical properties.

Conclusion: Based on these results, the ^{19}F NMR method was confirmed to be a convenient and useful tool for assessing the pharmacokinetics of LNEs without the need for complicated pretreatment procedures such as the deproteination of the matrix and extraction of the target compound before the ^{19}F NMR measurements.

Keywords: Lipid nano-emulsion; ^{19}F NMR; α-Tocopherol; Pharmacokinetics; Particle size; Zeta potential; Drug carrier

Introduction

Investigation of the pharmacokinetics of drug carriers in the body provides valuable information for drug delivery system (DDS) research. Fluorescent probes [1] and radioisotope-labeled molecular probes [2] are generally used for this purpose. Evaluation of drug carriers distributed in the blood and organs has been performed by quantitative determination of molecular probes loaded onto drug carriers in the blood and in each organ. However, the complicated tasks of deproteination of the matrix and extraction of the target compound must be completed before analysis using high-performance liquid chromatography (HPLC) can be carried out. Moreover, the radioactive nature of the radioisotopes makes human exposure a risk and necessitates the use of strict control measures in dedicated facilities. These complicated restrictions and pretreatment requirements interfere with the development of fast-acting, effective drug carriers.

^{19}F nuclear magnetic resonance (NMR) spectroscopy has the potential to be a powerful tool for pharmacokinetic studies of drug carriers. The usefulness of ^{19}F NMR can be attributed to the fact that the natural abundance of the ^{19}F nucleus is 100% and its sensitivity relative to protons is approximately 83%. In addition, the ^{19}F NMR chemical shift has a range of approximately 250 ppm, which is much greater than that of the ^{1}H NMR chemical shift; that is, ^{19}F NMR signals are more sensitive to changes in the chemical environment than ^{1}H NMR signals. Because the ^{19}F nucleus is not present in natural biological substances, it is easily detectable without interfering signals even in the presence of low concentrations of ^{19}F-containing compounds [3].

Lipid nanoparticles such as lipid emulsions (LEs), liposomes, solid lipid nanoparticles and micelles have been a focus of DDS research as they are physiologically compatible, targetable, generally non-toxic and amenable to large-scale production. Compared with other carriers, LEs have many advantages including that they exhibit a higher drug solubilization capacity that are easier to process and manufacture, and are more cost effective [4,5]. LEs are frequently used for safe administration of parenteral nutrition in clinical settings. Because LEs are expected to act as good drug carriers because of their high lipophilicity and apolarity, which allows them to cross cell membranes, they have also been used as parenteral DDS carriers [6] for sites of

***Corresponding author:** Shigehiko Takegami, Department of Analytical Chemistry, Kyoto Pharmaceutical University, 5 Nakauchicho, Misasagi, Yamashina-ku, Kyoto 607-8414, Japan, Tel: +81 75 5954659; Fax: +81 75 5954760; E-mail: takegami@mb.kyoto-phu.ac.jp

Received July 24, 2014; **Accepted** February 20, 2015; **Published** February 27, 2015

Citation: Takegami S, Katsumi H, Asai K, Fujii D, Fujimoto T, et al.(2015) Application of ^{19}F NMR Spectroscopy Using a Novel α–Tocopherol Derivative as a ^{19}F NMR Probe for a Pharmacokinetic Study of Lipid Nano-Emulsions in Mice. Pharm Anal Acta 6: 339. doi:10.4172/2153-2435.1000339

inflammation [7], as well as the heart [8] and lymphatic system [9], because of their tendency to accumulate in these areas. Moreover, recently, LEs have been employed as carriers of anticancer agents to improve their therapeutic indices and minimize drug cytotoxicity in normal cells [10-16]. It has been recognized that only drug carriers less than 100 nm in diameter can pass through the discontinuous capillary endothelium of tumors [17]. LEs with droplet sizes on the nanometer scale are characterized as lipid nano-emulsions (LNEs). LNEs with droplet sizes of less than 100 nm show high selectivity towards tumor tissues [18,19] because they accumulate passively because of leaky tumor vasculature. This is known as the enhanced permeation and retention (EPR) effect [20,21]. In a previous study, we developed an LNE that was prepared from a lipid mixture of soybean oil (SO), phosphatidylcholine (PC), sodium palmitate (PANa) and sucrose fatty acid ester [22]. As the mean droplet size of this LNE was approximately 50 nm, it was investigated as a DDS carrier for cancer therapy [23,24].

The aim of our study was to use ^{19}F NMR spectroscopy as an analytical technique to investigate the pharmacokinetics of LNEs. We focused on α-tocopherol (α-TP), a lipid-soluble vitamin with no reported adverse reactions, as the ^{19}F NMR probe compound. In this study, we synthesized a novel ^{19}F derivative of α-TP (^{19}F-TP) for use as a ^{19}F NMR probe by introducing a 4-(trifluoromethyl)benzoyl group to the hydroxyl group of α-TP, and used ^{19}F NMR to establish a procedure for convenient evaluation of LNE pharmacokinetics without the need for complicated pretreatment procedures.

Materials and Methods

Reagents and materials

α-TP and pyridine were purchased from Wako Pure Chemical Industries (Kyoto, Japan). 4-(Trifluoromethyl)benzoyl chloride, 4-(dimethylamino)pyridine, sodium palmitate (PANa) and bovine serum albumin (BSA, essentially fatty acid free) were purchased from Sigma-Aldrich (MO, USA). Deuterium oxide (D_2O), also purchased from Sigma-Aldrich, was used as the lock signal for ^{19}F NMR measurements. Soybean oil (SO) and glycerin were purchased from Kanto Chemical Co. (Tokyo, Japan). Egg yolk phosphatidylcholine (PC, COATSOME NC-50) with a purity of greater than 98% was supplied by NOF Co. (Tokyo, Japan) and used without further purification. 1, 2-Dipalmitoyl-*sn*-glycero-3-phosphatidylethanolamine-N-[methoxy (polyethylene glycol (PEG))-2000] (ammonium salt) (PEG-DPPE) was purchased from Avanti Polar Lipids, Inc. (AL, USA). Trifluoromethane sulfonic acid sodium salt (TFMS) was purchased from Kanto Chemical Co. (Tokyo, Japan). All other reagents were of analytical grade.

Chemical synthesis of ^{19}F-TP

The chemical reaction used in this study, which involves the benzoylation of a phenolic hydroxyl group, is shown in Figure 1. α-TP (2.00 g, 4.64 mmol), 4-(dimethylamino)pyridine (113 mg, 0.93 mmol) and 4-(trifluoromethyl)benzoyl chloride (1.52 mL, 10.21 mmol) were added to an empty 100-mL round-bottomed flask along with 50 mL of pyridine and the resulting suspension was stirred for 18 h at room temperature. Progress was monitored by silica gel thin-layer chromatography (TLC). The pyridine was removed using a rotary evaporator and the product was extracted with ethyl acetate. The resulting clear solution was washed with 3% HCl solution followed by saturated NaCl solution, and then dried over anhydrous Na_2SO_4, which was subsequently removed by filtration. Ethyl acetate was removed using a rotary evaporator, and the residue was purified by silica gel chromatography using hexane/ethyl acetate (30:1 v/v) to give white oil. The final product, ^{19}F-TP, was obtained in 96% yield. The purity of ^{19}F-TP was confirmed by ^{1}H NMR and TLC using hexane:ethyl acetate=30:1 (v/v). The retardation factor (R_f) of ^{19}F-TP was 0.3 by TLC.

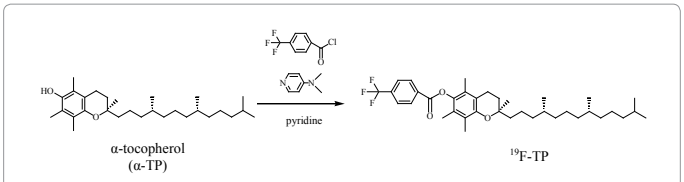

Figure 1: Synthesis of the α-tocopherol derivative ^{19}F-TP.

Preparation of ^{19}F-TP-LNEs

The formulations of the three LNEs containing ^{19}F-TP (Small-LNE, Large-LNE, and PEG-LNE), generalized as ^{19}F-TP-LNEs, are shown in Table 1. The preparation of spherical LNE particles was carried out using a sonication method that is described in detail elsewhere [22]. The mixture was emulsified by sonication using a VC-501 instrument (Tokyo Rikakikai Co. Ltd., Tokyo, Japan) for 1 h at 55°C in a thermostatic water bath. Sonication for 3 min was repeated at 3-min intervals. The ^{19}F-TP-LNE suspensions were centrifuged at 2000 × *g* to eliminate sediment from the sonication tip and then stored in tightly closed, light-resistant, glass containers at room temperature under a nitrogen atmosphere. The exact ^{19}F-TP concentrations in three ^{19}F-TP-LNE suspensions were measured using HPLC as indicated below. Analytical samples were dissolved in methanol before injection. All measurements were carried out in triplicate. The mean and standard deviation (S.D.) of ^{19}F-TP concentrations in three ^{19}F-TP-LNE suspensions were 27.3 ± 1.2, 27.5 ± 0.9, and 27.1 ± 0.8 mM for Small-LNE, Large-LNE and PEG-LNE, respectively.

Characterization of ^{19}F-TP-LNE preparations

The ^{19}F-TP-LNE preparations were further diluted with deionized-distilled water to 1:1000 for droplet size measurement and to 1:10,000 for zeta potential measurement. The mean diameters and droplet size distributions of the ^{19}F-TP-LNE particles were determined by dynamic light-scattering (DLS) using a Nicomp 380 analyzer (Particle Sizing Systems, Santa Barbara, CA, USA) and the ^{19}F-TP-LNE droplet size was reported as a volume-weighted distribution. Zeta potential values were measured using a Zeecom ZC-3000 analyzer (Microtec Co., Ltd., Chiba, Japan), based on the principle of electrophoresis.

Animals

Male specific-pathogen-free ddY mice (aged 5–6 weeks, 28-30 g) were purchased from Japan SLC Inc. (Shizuoka, Japan) and maintained under conventional housing conditions. All animal experiments were conducted in accordance with the principles and procedures outlined in the National Institutes of Health Guide for the Care and Use of Laboratory Animals. The protocols for animal experiments were approved by the Animal Experimentation Committee of Kyoto Pharmaceutical University.

A dose of 100 μL of each of the prepared ^{19}F-TP-LNE suspensions was injected into the mice via the tail vein. At selected intervals thereafter, the mice were lightly anesthetized, dissected and bled via the vena cava using a hypodermic needle treated with heparin, after which both the liver and kidney of the mice were excised and washed with saline.

^{19}F-TP-LNE	SO (g)	PC (g)	PANa (g)	PEG-DPPE (g)	^{19}F-TP (g)	Distilled water containing 2.2% glycerol (mL)
Small-LNE	0.7	0.168	0.0168	–	0.126	7
Large-LNE		0.084	0.0084	–		
PEG-LNE		0.168	0.0168	0.0064		

Table 1: Formulations of ^{19}F-TP-LNEs.

HPLC assay

A reverse-phase HPLC method was used for analysis of ^{19}F-TP. Quantitative determination of ^{19}F-TP in the analytical samples prepared from the ^{19}F-TP-LNE preparations and mouse plasma was performed by the absolute calibration method using a COSMOSIL 5C$_{18}$-MS-II column (4.6×150 mm, 5 μm, Nacalai Tesque Co., Kyoto, Japan) using methanol as a mobile phase at a flow rate of 1.0 mL/min. The injection volume of the analytical samples was 20 μL and ^{19}F-TP detection was performed using a ultraviolet detector at 280 nm. The t_R value of ^{19}F-TP was 16.7 min. This HPLC method was linear (R = 0.999) over a ^{19}F-TP concentration range of 5-100 μM. The lower limit of quantification (LLOQ) was set at 5 μM.

^{19}F NMR measurements

All ^{19}F NMR spectra were measured using a ^{UNITY}*INOVA* spectrometer (Agilent Technologies, Inc., Santa Clara, CA, USA) operating at 376.21 MHz without proton decoupling. The set parameters were a 3.0-μs pulse width (30° for the flip angle), a relaxation delay of 0.5 s, and an acquisition time of 0.5 s. The probe temperature was 25°C. The number of free induction decay (FID) accumulations to improve the signal-to-noise (S/N) ratio was from 1000 to 80,000, which corresponded to an accumulation time of approximately 16 min to 22 h.

Calibration curve of ^{19}F-TP from ^{19}F-TP-LNE in blood

Fresh blood taken from the vena cava of male ddY mice anesthetized with ether was used without removal of the blood cells. The calibration samples were prepared by adding 300 μL of blood suspension containing various amounts of ^{19}F-TP-LNE suspension to 240 μL of D_2O and 60 μL of a 1 mM TFMS-D_2O stock solution so as to achieve a concentration of *ca*. 0.1 mM TFMS. The samples were stirred and transferred into 5-mm-diameter NMR sample tubes, and ^{19}F NMR was carried out in triplicate at five suitable ^{19}F-TP concentrations under the conditions described above. A ^{19}F-TP calibration curve was prepared by plotting the ^{19}F-TP concentration on the horizontal axis and the ratio of the signal intensity of ^{19}F-TP to the signal intensity of the trifluoromethyl group of 0.1 mM TFMS, the internal standard, on the vertical axis.

Calibration curves of ^{19}F-TP from ^{19}F-TP-LNE in liver and kidneys

First, 1 mL of lysis buffer (0.1 M Tris/HCl, 0.05% Triton X100, and 2 mM EDTA, pH 7.8) was added to 1-g samples of liver or kidney. The organ suspensions were homogenized using a Physcotron NS-360 instrument (Microtec Co. Ltd., Chiba, Japan) at 30,000 rpm for 1 min, and were used without further separation such as centrifugation or filtration. To prepare calibration samples, 300 μL of the prepared organ suspension containing various amounts of ^{19}F-TP-LNE suspension was added to 240 μL of D_2O and 60 μL of a 1 mM TFMS-D_2O stock solution to achieve a concentration of *ca*. 0.1 mM TFMS. ^{19}F NMR measurements were carried out in triplicate at five suitable ^{19}F-TP concentrations under the conditions described above, and a ^{19}F-TP calibration curve was prepared in a manner similar to that described above.

Determination of ^{19}F-TP concentration in mouse blood using ^{19}F-NMR

At suitable time intervals, an analytical sample was prepared by adding a 300-μL blood sample from a mouse to 240 μL of D_2O and 60 μL of a 1 mM TFMS-D_2O stock solution to achieve a concentration of 0.1 mM, and ^{19}F NMR measurements were carried out using the conditions described above. ^{19}F-TP concentrations were calculated using the calibration curve described above.

Determination of ^{19}F-TP concentration in mouse plasma using HPLC

The blood samples from mice were centrifuged at 10,000 rpm (× 5500 *g*) for 5 min to give plasma samples, after which 100 μL of plasma was added to 900 μL of ultrapure water and 6 mL of ethyl acetate. After deproteination, the mixtures were centrifuged at 3500 rpm (× 2000 *g*) for 10 min. Thereafter, 5 mL of the upper layer was withdrawn from the mixture and dried at 60°C. The analytical samples were prepared by adding 100 μL of methanol to the residue. The ^{19}F-TP concentrations were measured using the HPLC experimental conditions described above.

Determination of ^{19}F-TP concentrations in mouse liver and kidneys using ^{19}F-NMR

At suitable time intervals, 1 mL of lysis buffer (0.1 M Tris/HCl, 0.05% Triton X100, 2 mM EDTA and pH 7.8) was added to 1-g samples of each organ, and the organ suspensions were homogenized at 30,000 rpm for 1 min. To prepare analytical samples, 300 μL of the prepared organ suspension was added to 240 μL of D_2O and 60 μL of a 1 mM TFMS-D_2O stock solution to achieve a final concentration of 0.1 mM. ^{19}F NMR measurements were carried out using the conditions described above. ^{19}F-TP concentrations for each organ were calculated using the calibration curve described above.

Results and Discussion

Chemistry

The novel compound (R)-2,5,7,8-tetramethyl-2-((4R,8R)-4,8,12-trimethyltridecyl)chroman-6-yl-4 (trifluoromethyl)benzoate (^{19}F-TP) was synthesized with a high yield of 96% in a one-step procedure as shown in Figure 1, in which a 4-(trifluoromethyl)benzoyl group was introduced to the hydroxyl group of α-TP in a widely used benzoylation reaction. The structure of the final product was verified by ^{1}H NMR spectroscopy. ^{1}H NMR (400 MHz, $CDCl_3$): δ 8.37 (br d, *J* = 8.6 Hz, 2H), 7.79 (br d, *J* = 8.6 Hz, 2H), 2.62 (t, *J* = 6.8 Hz, 2H), 2.13 (s, 3H), 2.05 (s, 3H), 2.01 (s, 3H), 1.88-1.70 (m, 1H), 1.82 (sep, *J* = 7.0 Hz, 1H), 1.64-1.05 (m, 21H), 1.26 (s, 3H), 0.87 (d, *J* = 7.0 Hz, 9H), 0.85 (d, *J* = 7.0 Hz, 3H).

Characterization of ^{19}F-TP-LNE preparations

The mean droplet sizes and zeta potential values of the three ^{19}F-TP-LNE preparations are shown in Table 2. The mean droplet sizes of the Small-LNE, Large-LNE and PEG-LNE were 58, 157 and 174 nm, respectively. The latter two values were comparable and approximately three times larger than that of the Small-LNE. The zeta potential of the Small-LNE was –34 mV, while that of the Large-LNE was lower at –53

^{19}F-TP-LNE	Diameter (nm)	Zeta potential (mV)
Small-LNE	58 ± 3	-34 ± 3
Large-LNE	157 ± 4	-53 ± 9
PEG-LNE	174 ± 4	-32 ± 2

Table 2: Particle size and zeta potential of ^{19}F-TP-LNEs (*n*=3).

mV. Using the mean droplet sizes of both LNEs, the total surface area of the Small-LNE droplets was calculated to be approximately three times as large as that of the Large-LNE droplets. The amount of PANa used for the preparation of the Small-LNE was twice that used for the Large-LNE as shown in Table 1. Thus, this difference was attributable to the larger total surface area of the Small-LNE droplet compared with the Large-LNE droplet, which resulted in a smaller amount of palmitate, which contains a COO^- group, per unit surface area. The zeta potential of the PEG-LNE, which had a similar droplet size to the Large-LNE, was –32 mV, which was comparable to the zeta potential of the Small-LNE. This may be the result of the fact that the surface of the PEG-LNE droplets, which was covered with a hydrophilic PEG layer, was not significantly influenced by the negative charge of the palmitate COO^- group [25].

^{19}F NMR spectroscopic behavior of ^{19}F-TP and ^{19}F-TP-LNE in the biological samples

The LNE particles interact with various biological substances in the body after administration. If ^{19}F-TP molecules localized at the PC/water interface of the LNE particles are pulled from the LNE particles by biological substances such as serum albumins and blood cells, this could prevent proper evaluation of the pharmacokinetics of LNE. For this reason, ^{19}F-NMR was used to examine the behavior of ^{19}F-TP in the LNE suspension and biological samples. Figure 2a shows the ^{19}F NMR spectrum of the Small-LNE containing 2 mM ^{19}F-TP in 100 mM phosphate buffer solution (pH 7.4). As shown in Figure 2a, a single sharp signal attributable to the trifluoromethyl group of ^{19}F-TP was observed at 15.4 ppm. In contrast, the signal of 2 mM ^{19}F-TP spiked with buffer solution containing bovine serum albumin (BSA) at a physiological concentration of 0.6 mM was shifted upfield to 14.9 ppm and considerably broadened as seen in Figure 2b. Because ^{19}F-TP is a highly lipophilic compound, the broadened signal is considered to be derived from ^{19}F-TP binding to BSA molecules. Meanwhile, the addition of 0.6 mM BSA to the Small-LNE buffer solution did not induce any significant changes in the chemical shift value of the ^{19}F-TP signal, i.e., 15.4 ppm, as depicted in Figure 2c. As shown in Figures 2a, 2b and 2c, the ^{19}F NMR signals of ^{19}F-TP in the Small-LNE suspension were not significantly different in the absence and presence of BSA, whereas ^{19}F-TP bound to BSA resulted in a clearly broadened signal that was shifted upfield. Thus, these results suggest that ^{19}F-TP may be localized in the inner SO phase of the Small-LNE particles and is not present in the water phase or on the lipid monolayer/water interface of the LNE particles where ^{19}F-TP can interact with BSA.

Figure 2d shows the ^{19}F NMR spectrum of the Small-LNE containing 2 mM ^{19}F-TP in a mouse blood suspension. A single sharp signal attributable to the trifluoromethyl group of ^{19}F-TP was observed at 15.4 ppm as shown in Figure 2d. The chemical shift value of this signal was similar to the corresponding signal in Figure 2a. In contrast, as seen in Figure 2e, the signal of free 2 mM ^{19}F-TP spiked in a blood suspension was considerably shifted downfield and slightly broadened at 16.50 ppm. The same results were also obtained for a liver suspension. This may have resulted from the single signal attributable to ^{19}F-TP interacting with the lipid membrane of blood cells and liver tissues. As indicated by the results in Figure 2d and 2e, the magnetic environment of ^{19}F-TP is different in the LNE particles and in the lipid membrane of biological cells, i.e., the presence of ^{19}F-TP can be detected by examining the ^{19}F NMR signal. To demonstrate the ^{19}F NMR spectroscopic behavior of ^{19}F-TP, further experiments were carried out. Figure 2f shows the ^{19}F NMR spectrum of both free 2 mM ^{19}F-TP and the Small-LNE containing 2 mM ^{19}F-TP spiked in a blood suspension. As seen in Figure 2f, two single signals were separately observed at 15.4 and 16.5 ppm, and are attributable to ^{19}F-TP in the Small-LNE and ^{19}F-TP interacting with the lipid membrane of blood cells, respectively. The same result was also obtained for the liver suspension. The spectral results indicate that the exchange rate of ^{19}F-TP between the two states in the LNE particles and in the blood cell membranes is slow on the ^{19}F NMR time scale. Therefore, if the ^{19}F-TP molecules are released from the LNE particles during blood circulation and organ accumulation, the signal at 16.5 ppm will be observed in the ^{19}F-NMR spectra for the biological samples.

^{19}F NMR spectra of ^{19}F-TP-LNE in blood

Figure 3 shows the ^{19}F NMR spectra of ^{19}F-TP in blood taken from the mice at 30, 60 and 360 min after the administration of the Small-LNE. A single sharp signal attributable to ^{19}F-TP was observed at 15.4 ppm in each spectrum, but was observed to decrease over time. As sedimentation of blood cells and LNE particles was not observed in all analytical samples after the ^{19}F NMR measurement, it was concluded that the condition of the blood samples could be maintained over long accumulation times, such as the 22 h required to improve the S/N ratio of the ^{19}F NMR spectra in the analytical samples at 360 min after administration.

The chemical shift values obtained from the spectral data at each time are shown in Table 3. The values obtained from the ^{19}F NMR spectra of the calibration samples used for preparation of the calibration curve are also shown in Table 3. These chemical shift values did not

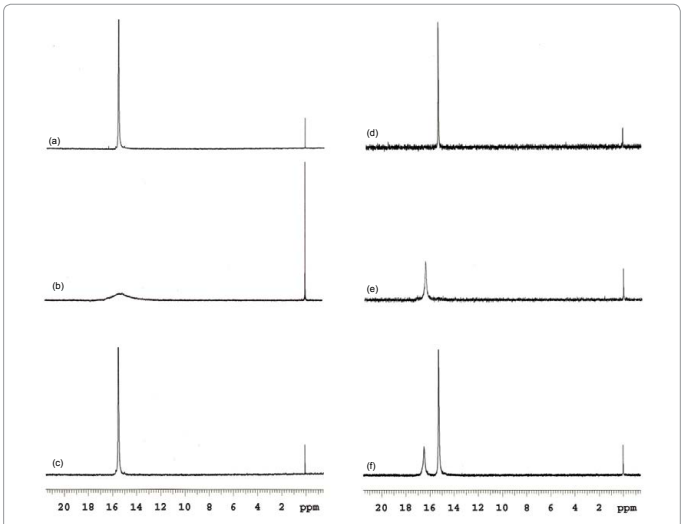

Figure 2: ^{19}F NMR spectra of the Small-LNE and/or free ^{19}F-TP in (a)–(c) 100 mM phosphate buffer solution (pH 7.4) and (d)–(f) mouse blood suspension. (a) Small-LNE (containing 2 mM ^{19}F-TP) without BSA, (b) 2 mM ^{19}F-TP with 0.6 mM BSA, (c) after the addition of 0.6 mM BSA to (a), (d) Small-LNE (containing 2 mM ^{19}F-TP) spiked with blood suspension, (e) 2 mM ^{19}F-TP spiked with blood suspension, (f) after the addition of both Small-LNE (containing 2 mM ^{19}F-TP) and 2 mM ^{19}F-TP to blood suspension. The internal reference (0 ppm) was 0.1 mM TFMS.

Sample	Time (min.)	Chemical shift (ppm)
Analytical samples[a]	5	15.42 ± 0.02
	15	15.40 ± 0.01
	30	15.40 ± 0.01
	60	15.40 ± 0.02
	180	15.44 ± 0.02
	360	15.44 ± 0.01
Calibration samples[b]		15.40 ± 0.04

Table 3: Chemical shift of the ^{19}F NMR signal of ^{19}F-TP in Small-LNEs in mice blood for analytical and calibration samples.
[a] Results are expressed as the mean ± S.D. (n=3).
[b] The triplicate measurements were carried out at five suitable concentrations of ^{19}F-TP for the preparation of the calibration curve. Results are expressed as the mean ± S.D. calculated from the total calibration samples (n=15).

change over time and were the same compared with the corresponding signals in Figure 2a and 2d. In addition, the signal attributable to the released ^{19}F-TP interacting with the blood cells observed at 16.50 ppm in Figure 2e was not observed in the ^{19}F NMR spectra for the analytical and calibration samples at any time. These results indicate that ^{19}F-TP was present in the same magnetic environment over time; that is, it did not leak from the Small-LNE particles and instead, remained encapsulated in them during blood circulation and the long ^{19}F NMR measurements. The signal intensity ratios of ^{19}F-TP to 0.1 mM TFMS were calculated and the calibration curve was used to quantitatively determine ^{19}F-TP. The curve showed good linearity (R = 0.998) over a ^{19}F-TP concentration range of 6-2800 μM. The LLOQ of ^{19}F-TP in blood was set at 6 μM.

Comparison of ^{19}F NMR and HPLC methods for examining the circulation of the ^{19}F-TP-LNE preparations

To confirm the usefulness of ^{19}F NMR as a convenient technique for assessing the pharmacokinetics of LNE, the ^{19}F-TP concentrations of the Small-LNE in blood and plasma were determined using ^{19}F NMR and traditional HPLC methods, respectively. The results are illustrated in Figure 4. There was a significant difference between the ^{19}F-TP concentration profiles determined using ^{19}F NMR and those determined using HPLC, and the concentrations obtained from the ^{19}F NMR method were similar to but higher than those obtained using the HPLC method. This is probably because during the extraction of ^{19}F-TP from the blood samples for HPLC analysis, no correction was made for any loss of ^{19}F-TP resulting from the extraction process. While the ^{19}F-TP concentration can be measured within approximately 20 min using the HPLC method (the t_R value of ^{19}F-TP is 16.7), complicated pretreatments such as deproteination, extraction and separation procedures are required before analysis. In contrast, using the ^{19}F NMR method, the ^{19}F-TP concentration can be easily obtained from intact blood samples without such complex procedures. However, there is still the need for time-consuming FID accumulations to improve the S/N ratio at lower ^{19}F-TP concentrations; e.g., for measurement of an analytical sample at 360 min, it takes more than 22 h to acquire a ^{19}F NMR spectrum with a S/N ratio sufficient to determine the quantity of ^{19}F-TP. In terms of applying this procedure to the measurement of biological samples with simple pretreatments, this result demonstrates that the ^{19}F NMR method is useful for determining the blood circulation of ^{19}F-TP-LNE.

Circulation of ^{19}F-TP-LNE preparations in blood

To examine whether ^{19}F NMR can detect different pharmacokinetics that may arise from the droplet size and surface physical properties of the LNE particles, the ^{19}F NMR spectra of three different ^{19}F-TP-LNEs (Small-LNE, Large-LNE, and PEG-LNE) in blood samples periodically bled from mice were determined and the corresponding ^{19}F-TP blood profiles were calculated. As shown in Figure 5, elimination of Large-LNE from the blood is almost complete 60 min after administration. More Small-LNE than Large-LNE is present in blood at 60 min, but the amount of Small-LNE decreases sharply from 42% to 12% from 30 to 60 min. We previously reported that Small-LNE flocculated in the presence of the counter ion Na^+ in saline and that the droplet size increased from 50 nm to 150 nm at more than 30 min after addition [22]. A rapid drop in the level of Small-LNE occurred when the droplet sizes increased in the presence of high concentrations of Na^+ in the blood. Approximately 8% of the amount of PEG-LNE administered remained in the blood 360 min later; the blood circulation of PEG-LNE was clearly better than those of the other two ^{19}F-TP-LNEs.

To quantitatively evaluate the differences in blood circulation among the three ^{19}F-TP LNEs, circulation data were calculated using MULTI [26], a nonlinear least-squares program based on a one-compartment model. The program was used to determine the areas under the blood concentration-time curves (AUCs) of the ^{19}F-TP-LNEs in Figure 5. It was found that the AUC of Small-LNE was 45.69

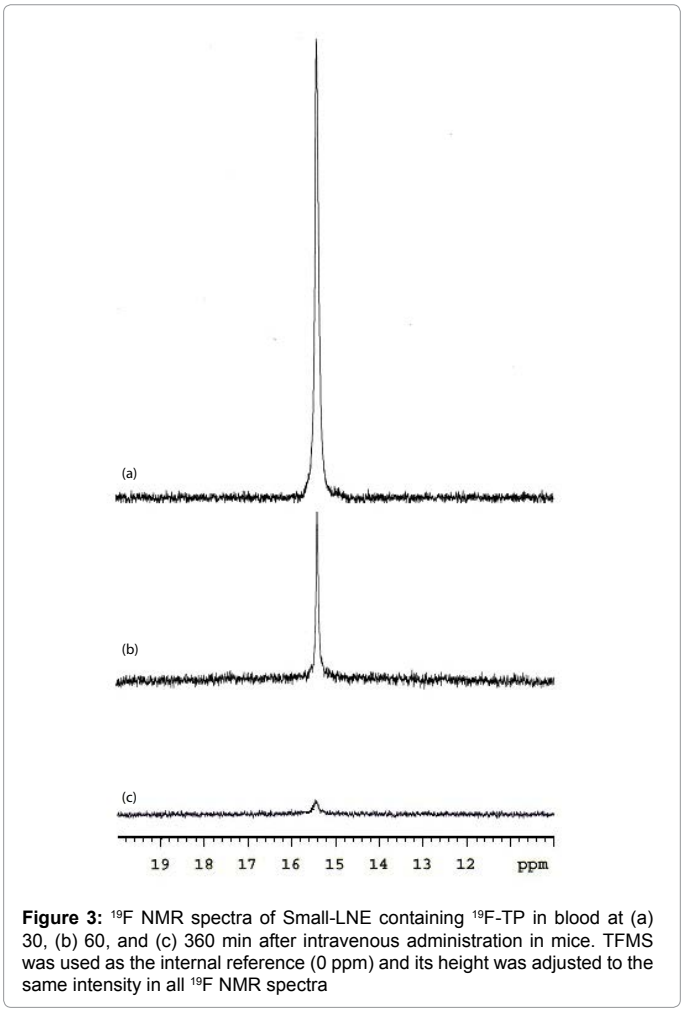

Figure 3: ^{19}F NMR spectra of Small-LNE containing ^{19}F-TP in blood at (a) 30, (b) 60, and (c) 360 min after intravenous administration in mice. TFMS was used as the internal reference (0 ppm) and its height was adjusted to the same intensity in all ^{19}F NMR spectra

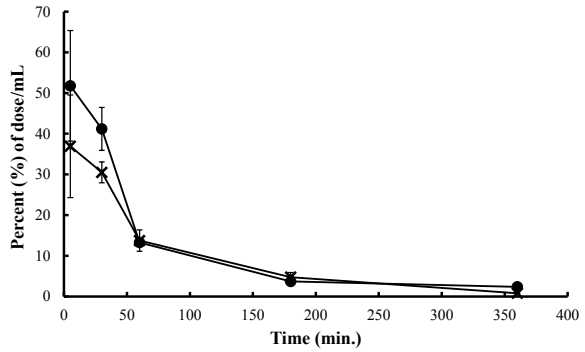

Figure 4: Blood and plasma concentration profiles of ^{19}F-TP determined by (●) ^{19}F NMR and (×) HPLC, respectively, after intravenous administration of Small-LNEs in mice. Each data point represents the mean ± S.D. for three mice.

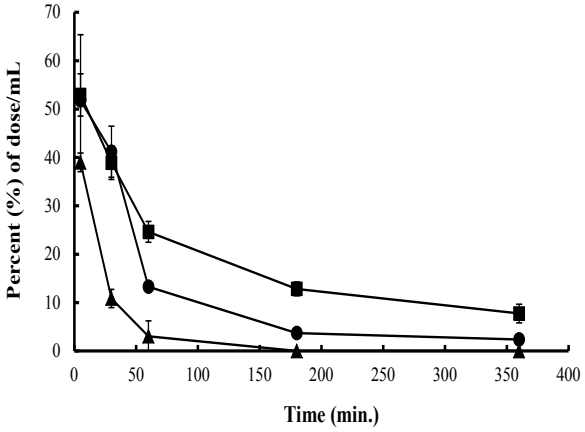

Figure 5: Blood concentration profiles of ^{19}F-TP determined by ^{19}F NMR after intravenous administration of (●) Small-LNE, (▲) Large-LNE, and (■) PEG-LNE in mice. Each data point represents the mean ± S.D. for three mice.

h·% of dose/mL, approximately 2.7-fold greater than that of Large-LNE at 16.64 h·% of dose/mL. It has been reported that physical and chemical properties such as particle size, surface charge and surface hydrophilicity are important in evaluating the biological fate of nanoparticles after intravenous administration [27,28]. LNEs disappear from the blood following uptake into the Kupffer cells of the liver, spleen macrophages and through other endocytotic processes of the reticuloendothelial system (RES). Larger mean droplet sizes are more easily captured by the RES [2,29]. Moreover, the degree of phagocytosis increases in proportion to the absolute zeta potential value [30,31]. On this basis, Large-LNE, which has a large droplet size and the smallest zeta potential value, was expected to have lower blood circulation than the Small-LNE. Thus, the LNEs are not captured by the RES and thus, they have increased blood circulation when the droplet size is sufficiently small. The AUC of PEG-LNE was 117.04 h·% of dose/mL, which was approximately 2.6 times greater than that of the Small-LNE, and the blood circulation time of PEG-LNE was greater than those of Small-LNE and Large-LNE despite its larger droplet size. The uptake of PEG into the RES is low because the substance has limited interactions with plasma proteins and cells [32-34]. The different blood circulation profiles of the three ^{19}F-TP-LNEs show ^{19}F-TP to be a useful ^{19}F NMR probe for evaluating LNE blood circulation.

Organ distribution of ^{19}F-TP-LNE preparations

^{19}F NMR was also used to determine the amount of ^{19}F-TP present in the livers and kidneys of mice. The calibration curve for each organ showed good linearity (R = 0.999) over a ^{19}F-TP concentration range of 6–2400 μM. The LLOQ of ^{19}F-TP in both organs was set at 6 μM. In addition, all of the chemical shift values of the analytical samples from both organs were unchanged compared with those in blood (Table 3). For example, the chemical shift was 15.44 ± 0.01 (ppm) in liver (N = 15), and 15.44 ± 0.01 (ppm) in kidney (N = 12), respectively. Furthermore, the signal at 16.4 ppm attributed to the released ^{19}F-TP interacting with the lipid membrane of organ cells as shown in Figure 2e was not observed in the ^{19}F NMR spectra for the analytical and calibration samples of both organs at any time.

The concentration profiles of the three ^{19}F-TP-LNEs in the liver and kidney are shown in Figure 6. The profiles of the ^{19}F-TP-LNEs in the liver correlated well with the obtained blood circulation profiles Figure 6a. As mentioned above, the Large-LNEs were eliminated from the blood just 30 min after administration. Its distribution in the liver at 30 min was approximately 14% and the concentration did not change subsequently. The uptake of both Small-LNE and PEG-LNE 30 min after administration was approximately 10%. At 60 min after administration, the Small-LNE distribution increased to 22%, compared with a distribution of approximately 15% for the PEG-LNE. This is explained by the finding that nanoparticles with diameters below approximately 70 nm will accumulate in the liver because of their penetration through the fenestrated endothelial lining [35]. The rapid increase in the Small-LNE distribution in the liver may also be attributed to the increase in LNE droplet size between 30 and 60 min after administration, which resulted in enhanced RES uptake in the Kupffer cells. The presence of PEG in the PEG-LNE resulted in a RES uptake that was lower than the distribution of the Small-LNE in the liver through a mechanism similar to that associated with the improved blood circulation of the PEG-LNE.

The distribution of the ^{19}F-TP-LNEs in the kidneys was relatively low Figure 6b, with the Small-LNE having the highest distribution. It is likely that the Small-LNE, with a mean droplet size of approximately 60 nm, had a greater renal uptake than the other LNEs because droplets in the 50-60 nm range are susceptible to interaction with the RES in the kidneys [36]. The renal distribution of the Large-LNE was low because a large proportion had already been taken up by the liver, while the renal distribution of the PEG-LNE was low because the presence of PEG excluded the LNE from the RES. The different concentration profiles of the three ^{19}F-TP-LNEs in the liver and kidneys show that ^{19}F-TP is a useful ^{19}F NMR probe for evaluating LNE distribution in various organs.

Conclusions

Differences in the droplet sizes and surface physical characteristics of the three ^{19}F-TP-LNEs resulted in differences in their blood circulation and organ distribution characteristics. This demonstrates the validity and usefulness of ^{19}F NMR as a convenient technique for assessing LNE pharmacokinetics. The use of ^{19}F-TP and ^{19}F NMR allows for convenient evaluation of LNEs and other drug carriers, and the results of this research should be useful in the development of fast-acting, effective drug carriers.

Acknowledgments

The authors thank Microtec Co. Ltd., for allowing us to use the homogenizer (Physcotron NS-360).

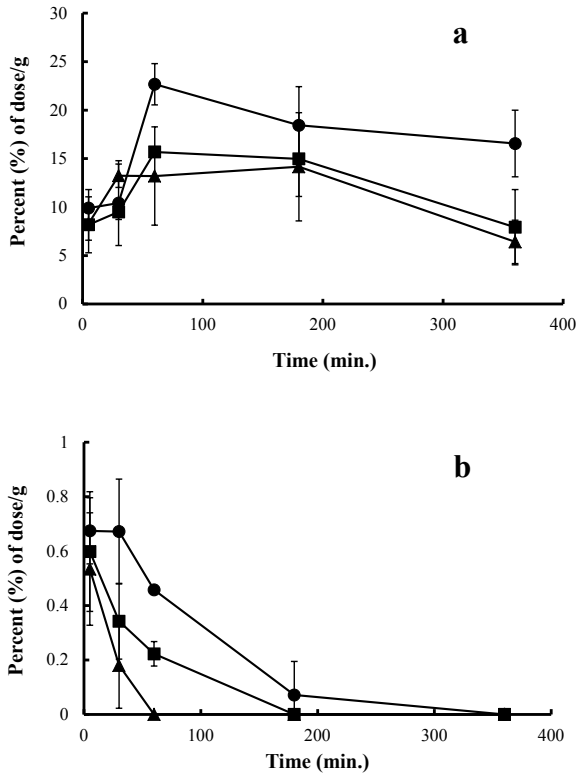

Figure 6: ^{19}F-TP concentration profiles in (a) liver and (b) kidney, determined by ^{19}F NMR after intravenous administration of (●) Small-LNE, (▲) Large-LNE, and (■) PEG-LNE in mice. Each data point represents the mean ± S.D. for three mice.

References

1. Janjic JM, Srinivas M, Kadayakkara DKK, Ahrens ET (2008) Self-delivering nanoemulsions for dual fluorine-19 MRI and fluorescence detection. J Am Chem Soc 130: 2832-2841.
2. Takino T, Konishi K, Takakura Y, Hashida M (1994) Long circulating emulsion carrier systems for highly lipophilic drugs. Biol Pharm Bull 17: 121-125.
3. Kitamura K, Omran AA, Takegami S, Tanaka R, Kitade T (2007) ^{19}F NMR spectroscopic characterization of the interaction of niflumic acid with human serum albumin. Anal Bioanal Chem 387: 2843-2848.
4. Lundberg BB, Mortimer B-C, Redgrave TG (1996) Submicron lipid emulsions containing amphipathic polyethylene glycol for use as drug-carriers with prolonged circulation time. Int J Pharm 134: 119-127.
5. Fukui H, Koike T, Nakagawa T, Saheki A, Sonoke S, et al. (2003) Comparison of LNS-AmB, a novel low-dose formulation of amphotericin B with lipid nano-sphere (LNS®), with commercial lipid-based formulations. Int J Pharm 267: 101-112.
6. Igarashi R, Takenaga M, Matsuda T (1996) Distribution of lipid microsphere preparations. Adv Drug Deliv Rev 20: 147-154.
7. Mizushima Y, Hoshi K, Aihara H, Kurachi M (1983) Inhibition of bronchoconstriction by aerosol of a lipid emulsion containing prostaglandin E1. J Pharm Pharmacol 35: 397.
8. Kimura A, Yamaguchi H, Watanabe K, Hayashi M, Awazu S (1986) Factors influencing the tissue distribution of coenzyme Q10 intravenous administered in an emulsion to rats: emulsifying agents and lipoprotein lipase activity. J Pharm Pharmacol 38: 659-662.
9. Sasaki H, Kakutani T, Hashida M, Sezaki H (1985) Absorption characteristics of the lipophilic prodrug of mitomycin C from injected liposomes or an emulsion. J Pharm Pharmacol 37: 461-465.
10. Kurihara A, Shibayama Y, Mizota A, Yasuno A, Ikeda M, et al. (1996) Enhanced tumor delivery and antitumor activity of palmitoyl rhizoxin using stable lipid emulsions in mice. Pharm Res 13: 305-310.
11. Nomura T, Koreeda N, Yamashita F, Takakura Y, Hashida M (1998) Effect of particle size and charge on the disposition of lipid carriers after intratumoral injection into tissue-isolated tumors. Pharm Res 15: 128-132.
12. Maranhão RC, Graziani SR, Yamaguchi N, Melo RF, Latrilha MC, et al. (2002) Association of carmustine with a lipid emulsion: in vitro, in vivo and preliminary studies in cancer patients. Cancer Chemother Pharmacol 49: 487-498.
13. Rossi J, Giasson S, Khalid MN, Delmas P, Allen C, et al. (2007) Long-circulating poly(ethylene glycol)-coated emulsions to target solid tumors. Eur J Pharm Biopharm 67: 329-338.
14. Kim SH, Kim JK, Lim SJ, Park JS, Lee MK, et al. (2008) Folate-tethered emulsion for the target delivery of retinoids to cancer cells. Eur J Pharm Biopharm 68: 618-625.
15. Zhao M, Su M, Lin X, Luo Y, He H, et al. (2010) Evaluation of docetaxel-loaded intravenous lipid emulsion: pharmacokinetics, tissue distribution, antitumor activity, safety and toxicity. Pharm Res 27: 1687-1702.
16. Trang P, Wiggins JF, Daige CL, Cho C, Omotola M, et al. (2011) Systemic delivery of tumor suppression microRNA mimics using a neutral lipid emulsion inhibits lung tumors in mice. Mol Ther 19: 1116-1122.
17. Wisse E (1970) An electron microscopic study of the fenestrated endothelial lining of rat liver sinusoids. J Ultrastruct Res 31: 125-150.
18. Seki J, Sasaki H, Doi M, Yoshikawa H, Takahashi Y, et al. (1994) Lipid nano-sphere (LNS), a protein-free analogue of lipoproteins, as a novel drug carrier for parenteral administration. J Control Release 28: 352-353.
19. Miyamoto M, Hirano K, Ichikawa H, Fukumori Y, Akine Y, et al. (1999) Preparation of gadolinium-containing emulsions stabilized with phosphatidylcholine-surfactant mixtures for neutron-capture therapy. Chem Pharm Bull 47: 203-208.
20. Matsumura Y, Maeda H (1986) A new concept for macromolecular therapeutics in cancer chemotherapy: mechanism of tumoritropic accumulation of proteins and the antitumor agent SMANCS. Cancer Res 46: 6387-6392.
21. Gabizon A, Papahadjopoulos D (1988) Liposome formulations with prolonged circulation time in blood and enhanced uptake by tumors. Proc Natl Acad Sci 85: 6949-6953.
22. Takegami S, Kitamura K, Kawada H, Matsumoto Y, Kitade T, et al. (2008) Preparation and characterization of a new lipid nano-emulsion containing two cosurfactants, sodium palmitate for droplet size reduction and sucrose palmitate for stability enhancement. Chem Pharm Bull 56: 1097-1102.
23. Takegami S, Kitamura K, Kawada H, Matsumoto Y, Yoshimura S, et al. (2013) Distribution of chloroaluminum phthalocyanine in a lipid nano-emulsion as studied by second-derivative spectrophotometry. Micro Nanosyst 2: 280-285.
24. Takegami S, Takara K, Tanaka S, Yamamoto K, Hori M, et al. (2010) Characterization, in vitro cytotoxicity and cellular accumulation of paclitaxel-loaded lipid nano-emulsions. J Microencapsul 27: 453-459.
25. Hashizaki K, Itoh C, Sakai H, Yokoyama S, Taguchi H, et al. (1999) Effects of PEG chain length of phospholipid with covalently attached poly(ethylene glycol) (PEG) on the macroscopic state of liposomes. J Jpn Oil Chem Soc 48: 871-876.
26. Yamaoka K, Tanigawara Y, Nakagawa T, Uno T (1981) A pharmacokinetic analysis program, (multi) for microcomputer. J Pharmacobio-Dyn 4: 879-885.
27. Tabata Y, Ikeda Y (1988) Effect of the size and surface charge of polymer microspheres on their phagocytosis by macrophage. Biomaterials 9: 356-362.
28. Awasthi VD, Garcia D, Goins BA, Phillips WT (2003) Circulation and biodistribution profiles of long-circulating PEG-liposomes of various sizes in rabbits. Int J Pharm 253: 121-132.
29. Takino T, Konishi K, Takakura Y, Hashida M (1993) Controlled biodistribution of highly lipophilic drugs with various parenteral formulations. J Drug Targeting 1: 117-124.
30. Gbadamosi JK, Hunter AC, Moghimi SM (2002) PEGylation of microspheres generates a heterogeneous population of particles with differential surface characteristics and biological performance. FEBS Lett 532: 338-344.
31. Xu F, Yuan Y, Shan X, Liu C, Tao X, et al. (2009) Long-circulation of hemoglobin-loaded polymeric nanoparticles as oxygen carriers with modulated surface charges. Int J Pharm 377: 199-206.

32. Woodle MC, Matthay KK, Newman MS, Hidayat JE, Collins LR, et al. (1992) Versatility in lipid compositions showing prolonged circulation with sterically stabilized liposomes. Biochim Biophys Acta 1105: 193-200.

33. Tobio M, Gref R, Sanchez A, Langer R, Alonso MJ (1998) Stealth PLA-PEG nanoparticles as protein carriers for nasal administration. Pharm Res 15: 270-275.

34. Li YP, Pei YY, Zhang XY, Gu ZH, Zhou ZH, et al. (2001) PEGylated PLGA nanoparticles as protein carriers: synthesis, preparation and biodistribution in rats. J Control Release 71: 203-211.

35. Litzinger DC, Buiting AMJ, Van Rooijen N, Huang L (1994) Effect of liposome size on the circulation time and intraorgan distribution of amphipathic poly(ethylene glycol)-containing liposomes. Biochim Biophys Acta 1190: 99-107.

36. Illum L, Davis SS (1982) The targeting of drug parenterally by use of microspheres. J Parenter Sci Technol 36: 242-248.